International Journal of Mathematical Analysis and Modelling

(Formerly Journal of the Nigerian Society for Mathematical Biology)

Volume 6, Issue 2 (Oct.-Nov.), 2023

ISSN (Print): 2682 - 5694
ISSN (Online): 2682 - 5708

Heat and mass transfer analysis of magnetohydrodynamic (MHD) thermosolutal nanofluid flow over vertical and inclined porous media

H. Nadab*†, S.A. Amoo†, and I.A. Olopade†

Abstract

In this study, the influence of heat and mass transfer on unsteady and steady MHD thermosolutal nanofluids flow in porous media in the presence of thermophoresis and Brownian motion effects was discussed. The governing boundary layer Partial Differential Equations (PDEs) were transformed into nonlinear Odinary Differential Equations (ODEs) by using similarity transformation and then solved numerically using fourth order Runge-Kutta method with shooting technique. It is found that increase in heat source (γ) and thermal conductivity (α) decreases the heat transfer rate but increases the skin friction and mass transfer rates. It is further discovered that the increase in thermal Grashof (G_r) and solutal Grashof (G_c) increases skin friction, heat and mass transfer rates.

Keywords: nanofluid; MHD; chemical reaction; radiation

1 Introduction

The combined study of heat and mass transfer of Magnetohydrodynamics (MHD) in the nanoparticules nanofluids is of great practical standing in engineering and sciences because of many branches of science and engineering using cooling application of nanofluids in manufacturing processes. There had been affordable amount of work carried out by scientist and researchers on radiative heat transfer in nanofluids due to their abundant applications. The study of MHD flow through porous media is encountered in a wide range of engineering and industrial applications such as extraction of crude oil, geothermal systems, thermal insulation, heat exchangers, packed bed analytic reactors, atmospheric and oceanic circulations e.t.c.

Heat and mass transfer analysis of Nanofluid flow based on Cu, Al2 O3, and T iO2 over a moving rotating plate and impact of various nanoparticle shapes was discussed [1]. Chemical reaction and thermal radiation effects on boundary layer flow of nanofluid over a wedge with viscous and Ohmic dissipation was investigated [2]. Cross-diffusion effects on heat and mass transfer of magnetohydrodynamic flow in porous media over exponentially stretching surface. They found out

*Corresponding Author
†Department of Mathematics and Statistics, Federal University Wukari, Taraba State, Nigeria

that solutal Grashof, thermal Grashof, magnetic parameter, radiation parameter, Dufour and Soret effects had significant effects on MHD fluid flow in porous media stretching surface was investigated [3]. Finite element Soret Dufour effects on an unsteady MHD heat and mass transfer flow past an accelerated inclined vertical plate was investigated [4]. Slip effects on heat and mass transfer in MHD Visco-Elastic fluid flow through a Porous Channel was analyzed [5]. Numerical approach of heat and mass transfer of MHD Casson fluid under radiation over an exponentially permeable stretching sheet with chemical reaction and Hall Effect was analyzed numerically [6]. Analytical and numerical solution of viscous fluid flow with the effects of thermal radiation and chemical reaction past a vertical porous surface was analyzed [7]. Computational frame work on MHD dissipative flow over a stretched region with cross diffusion simultaneous solutions was discussed [8].

Influence of novel turbulator on efficiency of solar collector system was presented [9] Numerical simulation of a time-dependent electroviscous and hybrid nanofluid with Darcy forchheimer effect between squeezing/compressing plates was investigated [10]. MHD and nonlinear thermal radiation effects on hybrid nanofluid past a wedge with heat source and entropy generation was presented [11]. Study of a nonuniform heat source over a Riga plate using nth order chemical reaction on Oldroyd-B nanofluid flow for two-dimensional motion was studied [12]. Influence of thermal radiation and viscous dissipation on MHD flow of UCM fluid over a porous stretching sheet with higher order chemical reaction was studied [13]. Maxwell nanofluid flow over an infinite vertical plate with ramped and isothermal wall temperature and concentration was discussed [14].

MHD flow of nano fluid past a vertical permeable semi-infnite moving plate with constant heat source was analyzed [15]. Computational treatment of Magnetohydrodynamics Maxwell nanofluid flow across a stretching sheet considering higher order chemical reaction and thermal radiation was computed [16].). Estimation of unsteady hydromagnetic Williamson fluid flow in a radiative surface through numerical and artificial neural network modeling was analyzed [17]. Statistical modeling for bioconvective tangent hyperbolic nanofluid towards stretching surface with zero mass flux condition was analyzed [18]. Non-linear thermal radiation and heat source effects on unsteady electrical MHD motion of nanofluid past a stretching surface with binary chemical reaction was investigated [19]. MHD non-Newtonian fluids flow past a stretching sheet under the influence of non-linear radiation and viscous dissipation was examined [20].

Analysis of heat and mass transfer of magnetohydrodynamics nanofluid flow in conducting feld through a vertical plate in porous medium was presented [21]. Radiation and chemical reaction effect on MHD thermosolutal nanofluid flow over a vertical plate in porous medium was suggested [22]. Impact of Lorentz Force and Viscous Dissipation on Unsteady Nanofluid Convection Flow over an Exponentially Moving Vertical Plate [23]. The exact solutions of time-dependent free convection MHD flow of some nanofluids close to a moving vertical plate, saturated in porous medium incorporating radiative heat flux and heat sink have been studied [24]. Analytical series solutions for the unsteady boundary layer flow of Williamson nanofluids induced by a permeable stretching sheet embedded in a porous medium in the presence of magnetic field, thermal radiation, and chemical reaction have been discussed [25].

Three dimensional nanofluid stirring with non-uniform heat source/sink through an elongated sheet was studied [26]. Simulation of time-dependent radiative heat motion over a stretching/shrinking sheet of hybrid nanofluid: Stability analysis for dual solutions was analyzed [27]. Impact of thermal conductivity on the thermophysical properties and rheological behavior of nanofluid and hybrid nanofluid was presented [28]. Impact of hybrid nanofluids on MHD flow and heat transfer near a vertical plate with ramped wall temperature have been studied [29]. Thermal

Radiation, Chemical Reaction and Viscous Dissipation Effects on Unsteady Magnetohydrodynamics (MHD) Flow of Viscoelastic Fluid Embedded in a Porous Medium was studied [30].

2 Formulation of the problem

Consider unsteady two-dimensional incompressible laminar boundary layer MHD flow of a viscous nanofuid over a permeable inclined stretching sheet. The nanofuid is supplied heat by the stretching sheet and concentration of chemical species at uniform rates. It is assumed that the influence of density variation with temperature and concentration occurs only on the body force term and hence the changes in both concentration and temperature induce the buoyancy force. A uniform magnetic Feld is applied normal to the surface of the stretching sheet. Further, it is assumed that a homogeneous first order chemical reaction with thermal radiation is taking place in the flow. It is assumed that the velocity of the stretching sheet is $u_w(x,t)$ in the direction of the force F applied along the x-axis and that of the mass transfer is $v_w(t)$ Normal to the stretched sheet.

It is also assumed that the surface wall temperature and concentration of the sheet are $T_w(x,t)$ and $C_w(x,t)$, respectively, while the uniform temperature and concentration far from the sheet are, respectively, T_∞ and C_∞. In addition, it is assumed that the efect described by Fourier's and Fick's law is of higher order of magnitude than the efect due to Dufour and Soret and thus the Dufour and Soret efects are neglected. The fluid thermal conductivity and molecular diffusivity are assumed to vary as a linear function of temperature. The model flow diagram is illustrated in Figure 1.

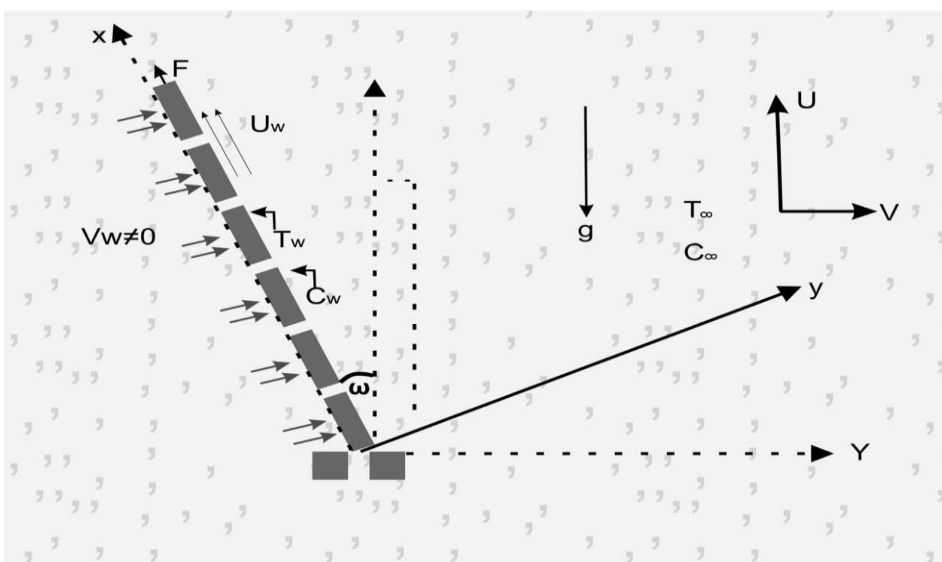

Figure 1: Physical Model and Coordinate system

Continuity equation

$$\frac{\partial u}{\partial x}+\frac{\partial v}{\partial y}=0, \tag{1}$$

Momentum equation

$$\frac{\partial u}{\partial t}+u\frac{\partial u}{\partial x}+v\frac{\partial u}{\partial y}=\mu\frac{\partial^2 u}{\partial y^2}-\frac{\sigma B_0^2 u}{\rho}-\frac{\mu}{K_p}u+g\beta_C\left(C-C_\infty\right)\cos\omega+g\beta_T\left(T-T_\infty\right)\cos\omega, \tag{2}$$

Energy equation

$$\frac{\partial T}{\partial t}+u\frac{\partial T}{\partial x}+v\frac{\partial T}{\partial y}=\alpha\frac{\partial^2 T}{\partial y^2}+\tau\left[D_B\frac{\partial C}{\partial y}\frac{\partial T}{\partial y}+\left(\frac{D_T}{T_\infty}\right)\left(\frac{\partial T}{\partial y}\right)^2\right]-\frac{1}{\left(\rho c_p\right)}\frac{\partial q_r}{\partial y}+\frac{Q}{\rho c_p}\left(T-T_\infty\right) \tag{3}$$

Concentration equation

$$\frac{\partial C}{\partial t}+u\frac{\partial C}{\partial x}+v\frac{\partial u}{\partial y}=D_B\frac{\partial^2 C}{\partial y^2}+\left(\frac{D_T}{T_\infty}\right)\left(\frac{\partial^2 T}{\partial y^2}\right)-\lambda\left(C-C_\infty\right). \tag{4}$$

The relevant boundary conditions are:

$$u=u_w(x,t)=\frac{cx}{1-\pi t},v=v_w(x,t),T=T_w(x,t),C=C_\infty(x,t)\ \text{at}\ y=0 \tag{5}$$

$$u\to 0,T\to T_\infty,C\to C_\infty\ \ \text{as}\ y\to\infty.$$

The radiation heat flux q_r is modelled using Rosseland's approximation which gives

$$q_r=-\frac{4\sigma^*}{3k^*}\frac{\partial 4T^4}{\partial y} \tag{6}$$

It is also assume that if the difference in the temperature within the flow is T^4, then T^4 can be written as the linear combination of the temperature by expanding T^4 by Taylor's series about T_∞ gives

$$T^4=T_\infty^4+4T_\infty^3\left(T-T_\infty\right)+6T_\infty^2\left(T-T_\infty\right)^2+\ldots \tag{7}$$

Neglecting the higher order beyond the first degree in $\left(T-T_\infty\right)$ then we have

$$T^4\approx -3T_\infty^4 T+4T_\infty^3 T, \tag{8}$$

where t is time, u is velocity in x direction, ρ is the Mass density of the fluid, C_P is Specific heat capacity at constant pressure, K_P is Permeability, λ is the Rate of chemical reaction, β_T is Coefficient of volumetric thermal expansion, β_C is Coefficient of volumetric expansion due to chemical species, T is Temperature of the species, C is Concentration of the species, T_∞ is Ambient temperature, C_∞ is Ambient concentration, μ is Kinematic viscosity of the ambient fluid, σ is Electrical conductivity, B_0 is Strength of external magnetic field, g is Acceleration due to gravity, q_r is Radiation heat flux, ω is Angle of inclination measured from the vertical axis to the stretching sheet, D_T is Thermophoretic diffusion coefficient, D_B is Brownian diffusion coefficient, c is Initial stretching sheet, w is Sheet ambient condition, ∞ is Boundary layer edge ambient condition, v_0 is Constant that describe the wall mass transfer parameter, σ^* is the Stefan-Boltzmann constant, k^* is Rosseland mean absorption coefficient, α is Thermal diffusivity of the fluid.

In other to transform the governing Partial Differential Equation (PDE), (2 - 4), will be transform into system of Ordinary Differential Equation (ODE) by introducing the dimensionless (similarity) variable given below

$$\eta = \sqrt{\frac{c}{\mu(1-\pi t)}}y, \psi(x,y) = \left(\frac{\mu c}{(1-\pi t)}\right)xf(\eta), \theta(\eta) = \frac{T-T_\infty}{T_w-T_\infty}, \phi(\eta) = \frac{C-C_\infty}{C_w-C_\infty}. \tag{9}$$

Therefore, $T = (T_w - T_\infty) + T_\infty$ and $C = (C_w - C_\infty) + C_\infty$.

Introducing the stream function $\psi(x,y)$ which define the velocity component in the form

$$u = \frac{\partial \psi}{\partial y}, v = -\frac{\partial \psi}{\partial x} \tag{10}$$

Using (10) in (1),

$$\frac{\partial}{\partial x}\left(\frac{\partial \psi}{\partial y}\right) - \frac{\partial}{\partial y}\left(\frac{\partial \psi}{\partial x}\right) = 0.$$

Continuity equation satisfies Cauchy Riemann equation, using (10) into (2) - (4), gives

$$\begin{aligned}\frac{\partial}{\partial t}\left(\frac{\partial \psi}{\partial y}\right) + \left(\frac{\partial \psi}{\partial y}\right)\left(\frac{\partial^2 \psi}{\partial x \partial y}\right) - \frac{\partial \psi}{\partial x}\left(\frac{\partial^2 \psi}{\partial y^2}\right) &= \mu\frac{\partial^3 \psi}{\partial y^3} - \frac{\sigma B_0^2}{\rho}\frac{\partial \psi}{\partial y} - \frac{\mu}{K_P}\frac{\partial \psi}{\partial y} \\ &\quad + g\beta_C(C-C_\infty)\cos\omega + g\beta_T(T-T_\infty)\cos\omega\end{aligned} \tag{11}$$

$$\frac{\partial T}{\partial t} + \frac{\partial \psi}{\partial y}\frac{\partial T}{\partial x} - \frac{\partial \psi}{\partial x}\frac{\partial T}{\partial y} = \alpha\frac{\partial^2 T}{\partial y^2} + \tau\left[D_B\frac{\partial C}{\partial y}\frac{\partial T}{\partial y} + \frac{D_T}{T_\infty}\left(\frac{\partial T}{\partial y}\right)^2\right] - \frac{1}{\rho C_P}\frac{\partial q_r}{\partial y} + \frac{Q}{\rho C_P}(T-T_\infty) \tag{12}$$

$$\frac{\partial C}{\partial t} + \frac{\partial \psi}{\partial y}\frac{\partial C}{\partial x} - \frac{\partial \psi}{\partial x}\frac{\partial C}{\partial y} = D_B\frac{\partial^2 C}{\partial y^2} + \frac{D_T}{T_\infty}\left(\frac{\partial^2 T}{\partial y^2}\right) - \lambda(C - C_\infty) \tag{13}$$

In view of similarity variable (9) on equations (11) – (13) the following equation (14) to (16) were obtained

$$f''' - A\frac{\eta}{2}f'' - (M+\varphi)f' - (f')^2 + ff'' + G_C\phi + G_r\theta = 0 \tag{14}$$

$$\left(1+\frac{4}{3\alpha}R\right)\theta''+\left[N_b\phi'-P_r\left(A\frac{\eta}{2}-f\right)\right]\theta'+N_t(\theta')^2+P_r\gamma\theta=0\,, \tag{15}$$

$$\phi''-L_e\left(A\frac{\eta}{2}-f\right)\phi'+\frac{N_t}{N_b}\theta''-L_e\delta\phi=0 \tag{16}$$

The relevant boundary conditions are

$$f(0)=f_w,\ f'(0)=0.3,\theta(0)=0.3,\phi(0)=0.3,\ f'(5)=0,\theta(5)=0,\phi(5)=0 \tag{17}$$

where prime denotes differentiation with respect to η. The dimensionless parameter describing they physical properties that is affected by temperature, is defined as follows

$A=\frac{\pi}{c}$ is the unsteadiness parameter, $\varphi=\frac{\mu(1-\pi t)}{cK_P}$ is the porous medium parameter, $M=\frac{\sigma B_0^2(1-\pi t)}{c\rho}$ is the magnetic parameter, $R=\frac{4T_\infty^3\sigma^*}{3k^*\rho c_p}$ is the thermal radiation parameter, $\delta=\frac{\lambda(1-\pi t)}{c}$ is the chemical reaction parameter, $G_r=\frac{g\beta_T x(T_w-T_\infty)\cos\alpha}{u_w^2}$ is the thermal Grashof number, $G_C=\frac{g\beta_C x(C_w-C_\infty)\cos\alpha}{u_w^2}$ is the concentration or solutal Grashof number, $N_b=\frac{\tau D_B(C_w-C_\infty)}{\alpha}$ is the Brownian motion parameter, $N_t=\frac{\tau D_T(T_w-T_\infty)}{\alpha T_\infty}$ is the thermophoresis parameter, $P_r=\frac{\mu}{\alpha}$ is the Prandtl number, $L_e=\frac{\mu}{D_B}$ is the Lewis number and $\gamma=\frac{Q(1-\pi t)}{c\rho c_p}$ is the heat source parameter.

3 Method of solution

The governing equations of heat and mass transfer effects on unsteady MHDs thermosolutal nanofliud flow are essentially PDEs transformed into nonlinear ODEs together boundary conditions are numerically solved using a computer embedded software code. The codes being of Runge-Kotta scheme with shooting techniques. This method has been proven to be adequate and seems to give accurate results and has be widely used [33], [34]. It seems to be the most flexible of the common methods. The scheme is also applicable to various types of boundary layer flow problems including the free and mixed connection flows.

In the numerical method employed in solving the model equations that is boundary value problem (BVP). Shooting techniques was also applied, this shooting techniques reformulates the BVP to initial value problem (IVP) by adding sufficient number of conditions at one end and adjust their conditions until the given condition are satisfied at the other end while Runge-Kutta method solve the initial value problem.

Equation (14) to (16) were integrated as IVPs the values for $f'''(0), \theta'(0)$ and $\phi'(0)$ which were required to explain the skin friction, Nusselt and Sherwood numbers, but no such value exist at the boundary. The suitable guess values for $f''(0), \theta'(0)$ and $\phi'(0)$ were chosen and then intergration was carried out. The researchers compared the calculated values for $f''(0), \theta'(0)$ and $\phi'(0)$ at η =5 with the given boundary conditions $f''(5)=0, \theta'(5)=0$ and $\phi'(5)=0$. Then the adjusted and the estimated values for $f''(0), \theta'(0)$ and $\phi'(0)$, to give a better approximation for the solution. The researchers transform a series of computations to obtain values for $f''(0), \theta'(0)$ and $\phi'(0)$ and then applied a fourth order Runge-Kutta with shooting techniques with step size h = 0.01. The above procedure was repeated until the results came up the desired degree of accuracy (10^{-6})

The computation to obtain velocity, temperature and concentration profiles were presented to observe the effect on heat and mass transfer of unsteady MHDs thermophoresis on porous media. The proportional effects on the skin friction coefficient, Nusselt and Sherwood numbers were presented and determined for independent parameters. To explain the effect on heat and mass transfer of unsteady MHDs thermophoresis in porous media.

Quantities of physical and practical interest in this model are the skin or local friction factor (C_f) which represent the wall shear stress physically, the Nusselt or local Nusselt number (Nu_x) which defines the heat transfer rate physically and Sherwood or local Sherwood number (Sh_x) which defines the mass transfer rates which are represented as follows

$$
\begin{aligned}
&C_f = \frac{2\tau_m}{\rho u_w^2},\ Nu_x = \frac{xq_w}{K(T_w - T_\infty)},\ Sh_x = \frac{xh_m}{D_B(C_w - C_\infty)} \\
&\tau_m = \mu\left[\frac{\partial u}{\partial y}\right]_{y=0},\ q_w = -K\left[\frac{\partial T}{\partial y}\right]_{y=0},\ h_m = -D_B\left[\frac{\partial C}{\partial y}\right]_{y=0}
\end{aligned}
\tag{18}
$$

In which τ_m, q_w *and* h_m are the skin friction or shear stress, heat flux and mass flux from the sheet respectively. The skin friction, heat flux and mass flux are as follow $f''(0) = \frac{1}{2}\sqrt{\mathrm{Re}_x}C_f,\ -\theta'(0) = \frac{Nu_x}{\sqrt{\mathrm{Re}_x}},\ -\phi'(0) = \frac{Sh_x}{\sqrt{\mathrm{Re}_x}}$ Where $f''(0)$ is the skin friction, $-\theta'(0)$ is the Nusselt number and $-\phi'(0)$ is Sherwood number, this also implies that $\mathrm{Re}_x = \frac{u_w x}{\mu} = \frac{cx^2}{\mu(1-\pi t)}$ is the local Reynolds number.

4 Results and discussion

Table 1 represents the results of variation in Skin friction ($f''(0)$), Nusselt ($-\theta'(0)$) and Shearwood numbers ($-\phi'(0)$) at the surface with magnetic field parameter M, thermal Grashof number Gr, solutal or concentration Grashof number Gc, porosity at the wall f_w, Lewis number Le, thermal diffusivity α, chemical reaction δ, porous medium parameter φ, heat source γ, unsteadiness parameter A, radiation parameter R, Prandtl number Pr, which are of physical and engineering interest. Also the friction factor, local Nusselt and Sherwood numbers are discussed and presented through graphs and tables. The computation was carried out using shooting technique with Runge-Kutta iteration algorithm. These were used for couple nonlinear differential equations along with boundary conditions. In the numerical solution, a check was to confirm that smoothness conditions at the end of boundary layer were satisfied. For numerical computations and results we consider the non-dimensional parameter, with their values as follows M = 1, Gr = Gc, f_w, Le, α =1, δ = φ = γ = A = R = 0.5, and Pr = 0.4, These values are considered to be constant throughout the entire research apart from the varied parameters shown in the figures.

Table 1: Numerical Approximation of the variation of parameters for $f''(0)$, $\theta'(0)$ and $\phi'(0)$

Parameter	Value	$f''(0)$	$-\theta'(0)$	$-\phi'(0)$
M	1	-0.048178	0.002663	0.223047
	4	-0.421512	-0.002680	0.212712
	5	-0.506547	-0.003437	0.210965
	7	-0.650434	-0.004452	0.208458
Gr	1	-0.044105	-0.025930	0.243175
	2.5	0.260343	-0.014428	0.250429
	3.5	0.450256	-0.008271	0.254167
	4.5	0.632298	-0.002930	0.257425
Gc	1	-0.044105	-0.025930	0.243175
	2.5	0.146030	-0.023193	0.247264
	3.5	0.269669	-0.021504	0.249778
	4.5	0.391145	-0.019900	0.252147
δ	0.5	-0.050851	-0.025757	0.279489
	1.5	-0.070576	-0.025074	0.413780
	2.5	-0.081585	-0.024661	0.513373
	3.5	-0.089143	-0.024388	0.596295
P_r	0.4	-0.044105	-0.025930	0.243175
	0.6	-0.034778	-0.089996	0.287858
	0.8	-0.017374	-0.204832	0.366537
	1	0.024284	-0.480675	0.555269

A	0.5	-0.044105	-0.025921	0.243175
	1.5	0.003179	-0.065406	0.186526
	2.5	0.028169	-0.088219	0.142952
	3.5	0.034934	-0.089555	0.116856
N_t	1	-0.044105	-0.025930	0.243175
	1.5	-0.053829	-0.029337	0.275758
	2	-0.064592	-0.032868	0.310066
	2.5	-0.076451	-0.036566	0.346120
N_b	1	1.361810	-0.019137	0.290769
	1.5	1.379045	-0.020744	0.272715
	2	1.389212	-0.022384	0.263783
	2.5	1.396505	-0.023912	0.258457
γ	0.5	-0.044105	-0.025930	0.243175
	0.8	-0.032522	-0.104795	0.297968
	1.1	-0.005723	-0.274607	0.412213
	1.3	0.081609	-0.821827	0.776237
φ	0.5	-0.044105	-0.025930	0.243175
	0.8	-0.096387	-0.027640	0.241806
	1.1	-0.143615	-0.029648	0.240580
	1.4	-0.186770	-0.030267	0.239477

Figures 2-4 present the influences of magnetic field parameter (M) on velocity, temperature and concentration profile respectively of the flow. It is evident from the figure 2 that an increase in the magnetic field parameter causes a decrease in the fluid velocity and 3 and 4 improves the distribution of temperature and concentration profile. It is due to the fact that an increase in magnetic field develops the force opposite to the direction of flow. But this force reduces the thermal and concentration boundary thickness, in this case, we see enhancement in the temperature and concentration profile.

Figures 5 - 7 shows the effect of thermal Grashof number (G_r) it is evident that increase in thermal Grashof parameter increases both nanofluid velocity, temperature and concentration profile. It was discovered that nanofluid velocity increased with increase in thermal Grashof parameter. This rely on the fact that thermal Grashof parameter is the ratio of thermal buoyancy force to the hydrodynamic force and this take place on the boundary layer due to changes in temperature and thus an increase in the thermal buoyancy effect on the nanofluid makes the fluid to cool the hot sheet, in this case thermal Grashof parameter slows down temperature and concentration.

Figures 8 - 10 display the effects of solutal Grashof parameter on fluid velocity, temperature and concentration profile respectively. The influence of solutal Grashof parameter on nanofluid velocity as shown in figure 8 shows that increase in solutal Grashof parameter increases the velocity profiles.

The values of temperature and concentration profile is increased due to variation in solutal Grashof parameter. In this case, temperature and concentration at the boundary layer gets thinner as solutal Grashof parameter increased.

Figures 11 - 13 illustrates the effect of chemical reaction parameter (δ) on velocity, temperature and concentration profile of the flow. It is evident that increase in δ decline nanofluid velocity flow thereby leds to increase in temperature and concentration profile. Figure 13 show that as δ increase, the concentration profile increases. Figure 14 – 16 present the influence of Prandtl number parameter (P_r) on velocity profile shown in figure 14 it can be noted that as the variation in P_r increases, the nanofluid velocity flow increases. It is important to note that from figure 15 P_r increases, it causes decrease in temperature of nanofluid, this is as a result that P_r is inversely proportional to the thermal diffusion and directly proportional to the momentum diffusivity and thereby as P_r incrases, it lead to the thermal diffusion and concentration of the fluid increases.

Figures 17 – 19 depicts the typical effect of unsteadiness parameter (A) on velocity, temperature and concentration profiles of the fluid flow, respectively. It is observed that increase in A decreases the temperature and concentration profiles of the flow. It was discovered that there is increase in the nanofluid velocity flow. It is also evident that increase in unsteadiness parameter increases the temperature close to the stretching sheet thereby the wall temperature is higher than the temperature of the surrounding, and as a result of high wall temperature nanoparticles move to cooler area, resulting in the decrease of the concentration profiles.

Figures 20 – 22 present the effects of thermophoresis parameter (N_t) on velocity, temperature and concentration profile of the nanofluid flow. Increase in N_t decreases the temperature profile and causes increase in concentration profile. Figure 23 – 25 illustrate the influence of Brownian motion parameter (N_b) on velocity, temperature and concentration profile of the flow. It is also discovered the increase in N_b causes increase in the nanofluid velocity and also leads to decrease in temperature and concentration profile. It is also observed that enhancement in the N_b result in the increment of velocity, temperature and concentration boundary layer thickness. Figure 26 – 28 exhibit the effects of heat source parameter (γ) on the velocity, temperature and concentration profile of the flow respectively. It is clear that an increase in the γ increase the nanofluid velocity and concentration profile of the flow, but a decrease in temperature profile is evident. The negative values of γ act as heat absorption.

Figures 29 – 31 illustrate the effects porous medium parameter (φ) on nanofluid velocity, temperature and concentration profile. It is clear that as φ increases, the non-dimensional velocity decline this is due to the fact that as the tightness of the tightness of φ increases, the resistance against the flow increases in this case the fluid velocity decreases and in this way the heat transferred from the plate. It is evident that the distribution of porous medium parameter enhance the temperature and concentration boundary layer thickness.

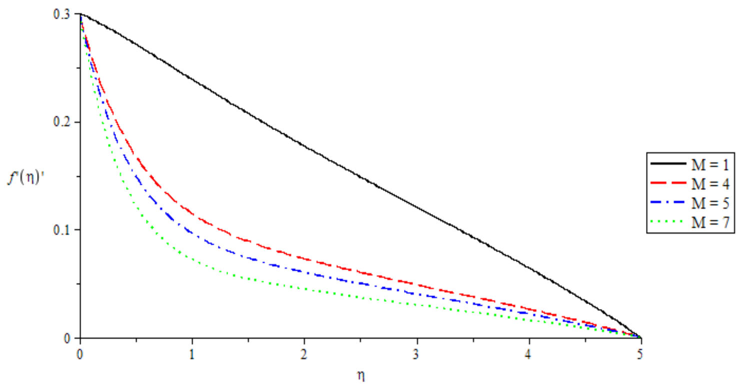

Figure 2: Variation of Hartmann number (M) on velocity profile

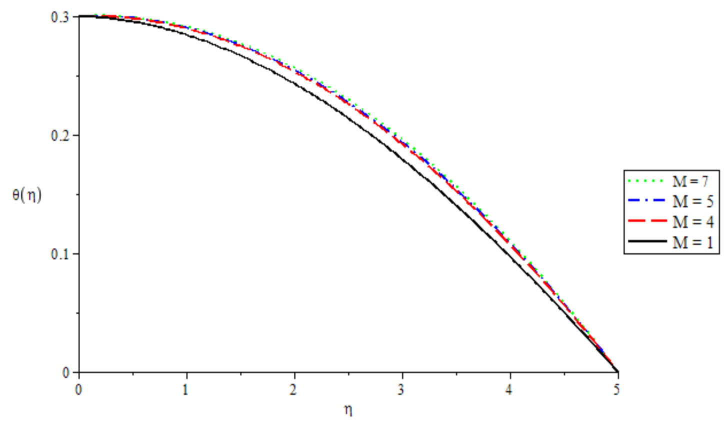

Figure 3: Variation of Hartmann number (M) on temperature profile

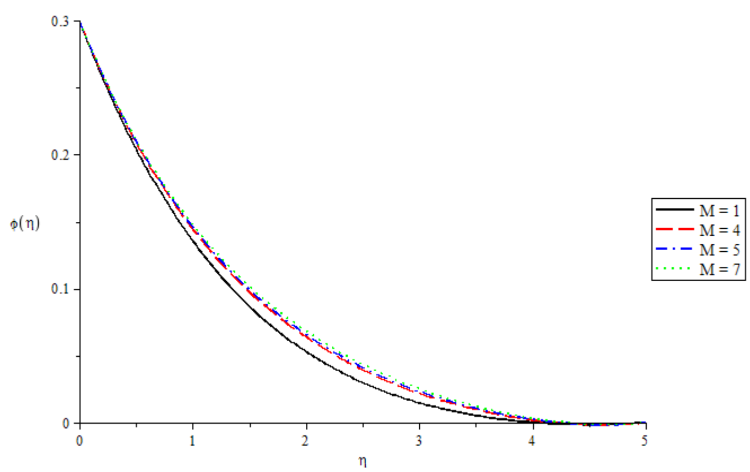

Figure 4: Variation of Hartmann (M) on concentration profile

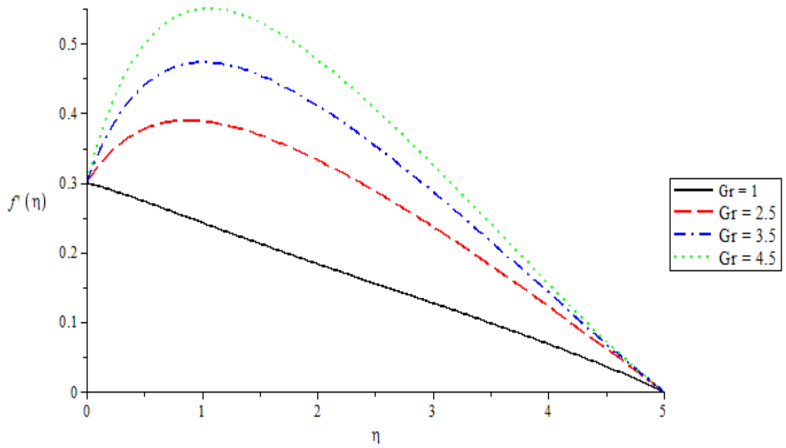

Figure 5: Variation of thermal Grashof number (G_r) on velocity profile

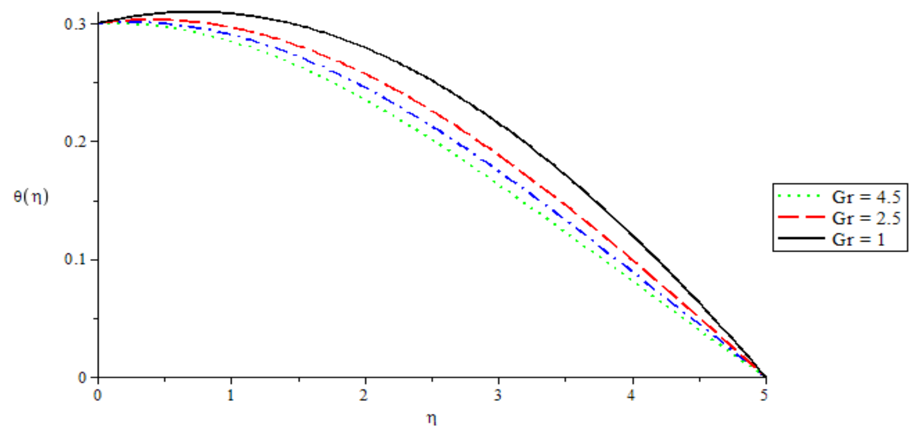

Figure 6: Variation thermal Grashof number (G_r) on temperature profile

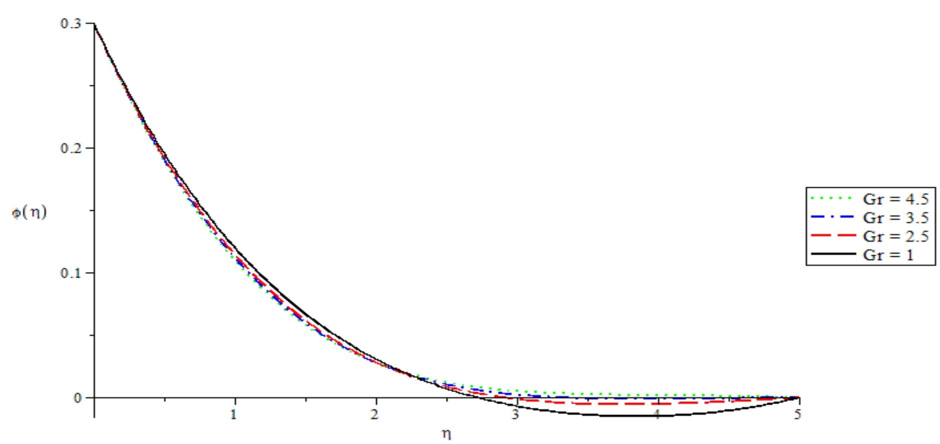

Figure 7: Variation of thermal Grashof number (G_r) 0n concentration profile

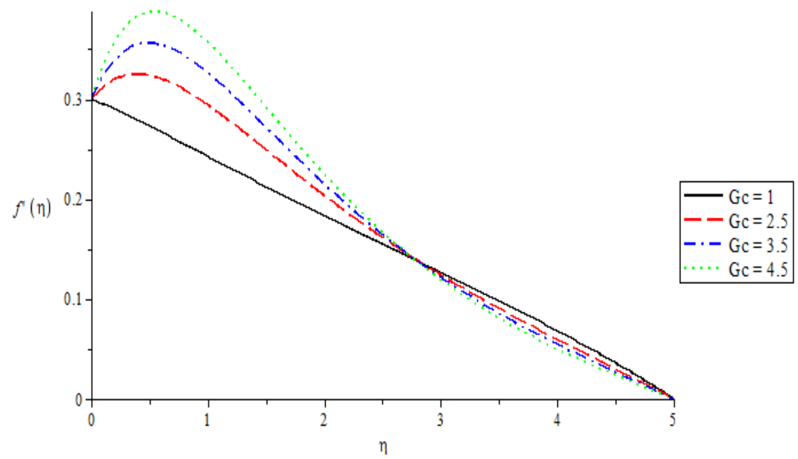

Figure 8: Variation of mass Grashof number (G_c) on velocity profile

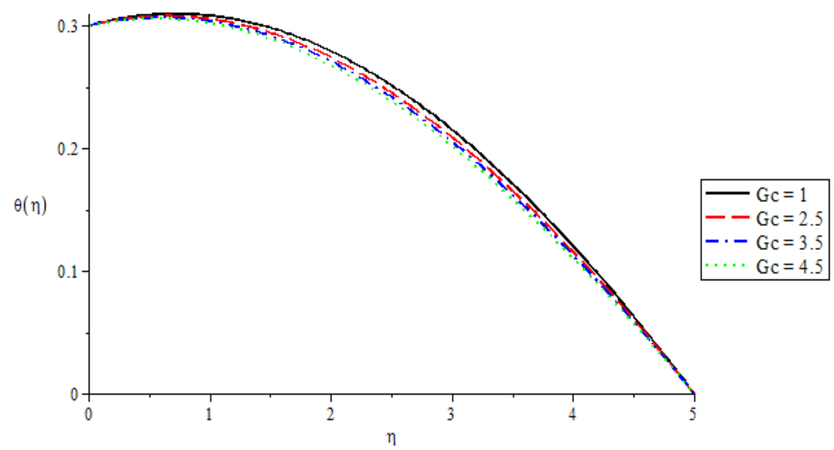

Figure 9: variation of mass Grashof number (G_c) on temperature profile

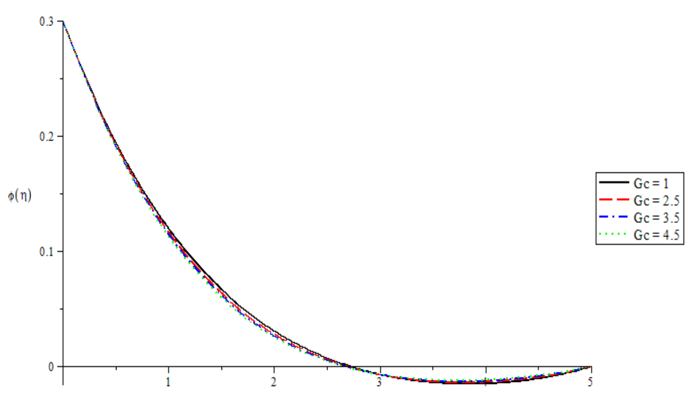

Figure 10: Variation of mass Grashof number (G_c) on concentration profile

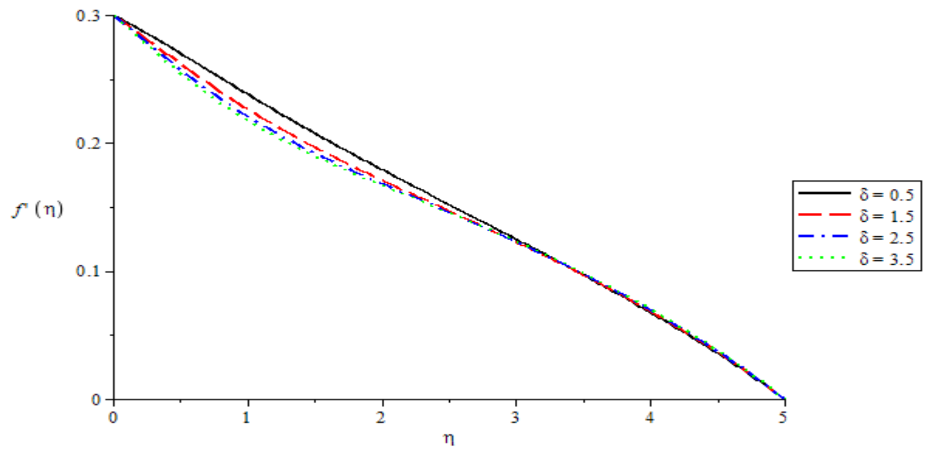

Figure 11: Variation of chemical reaction (δ) on velocity profile

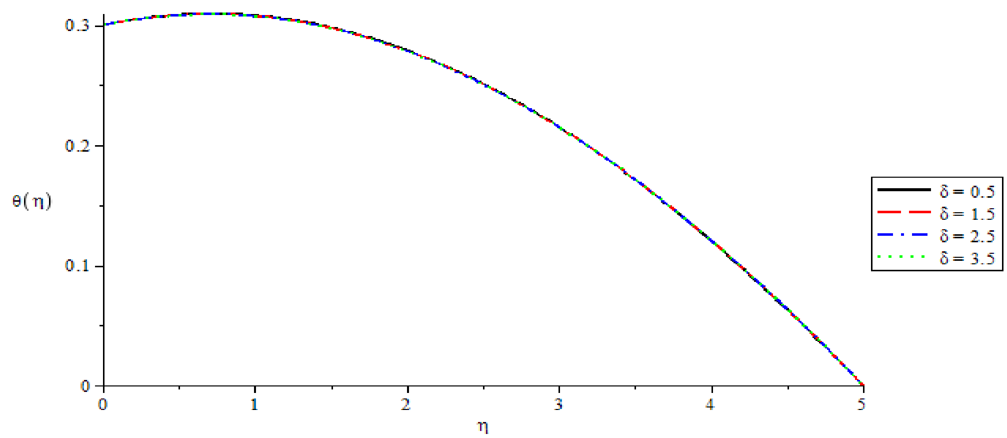

Figure 12: Variation of chemical reaction (δ) on temperature profile

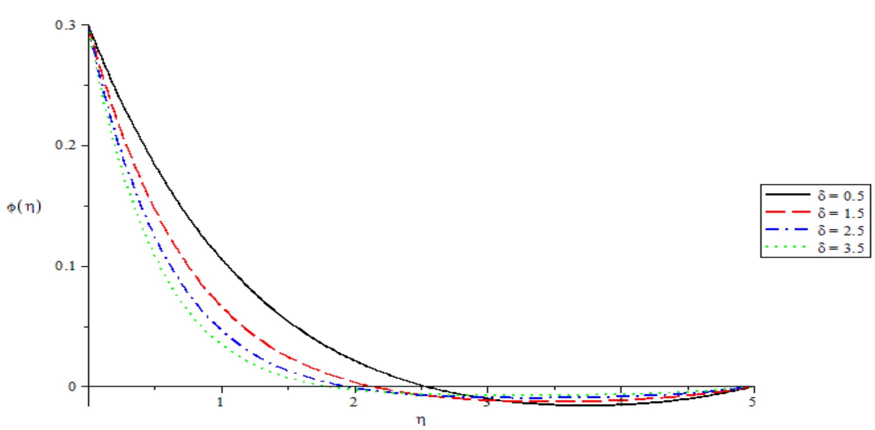

Figure 13: Variation of chemical reaction (δ) on concentration profile

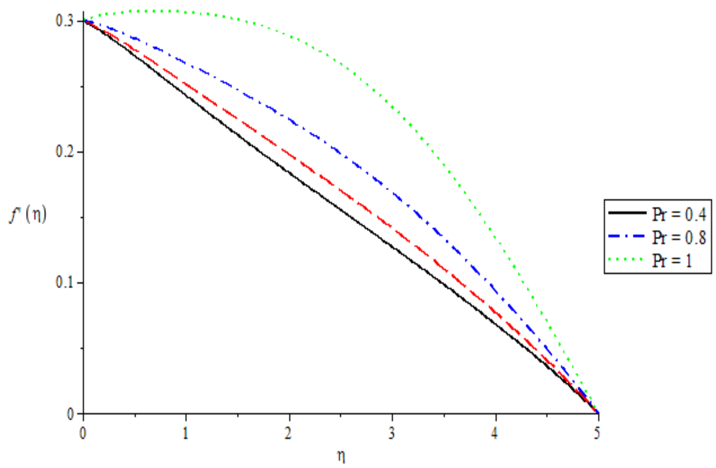

Figure 14: Variation of Prandtl number (P_r) on velocity profile

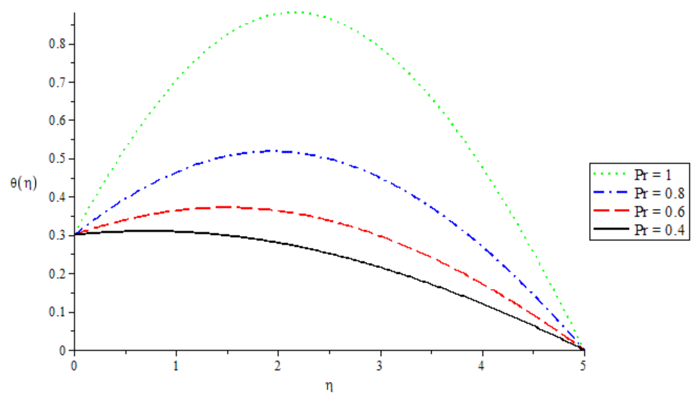

Figure 15: Variation of Prandtl number (P_r) on temperature profile

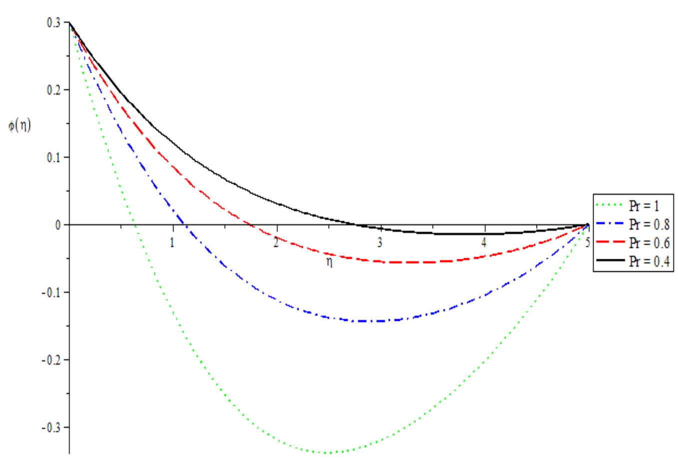

Figure 16: variation of Prandtl number (P_r) on concentration profile

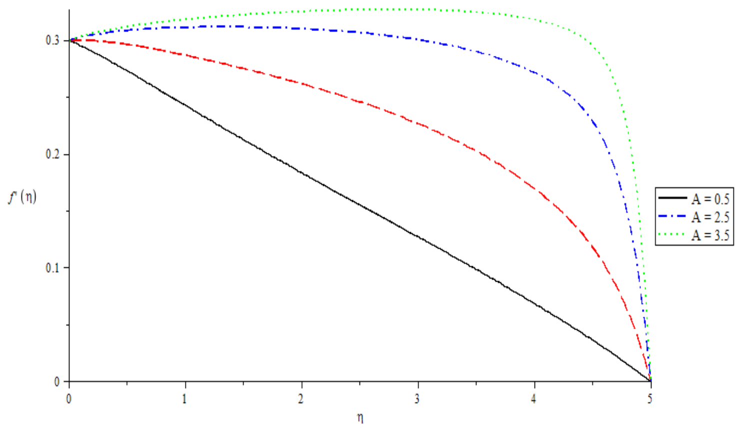

Figure 17: Variation of unsteadiness parameter (A) on velocity profile

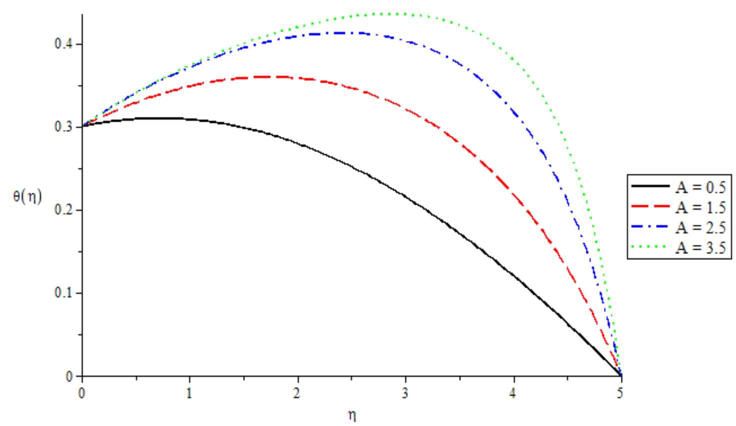

Figure 18: Variation of unsteadiness parameter (A) on temperature profile

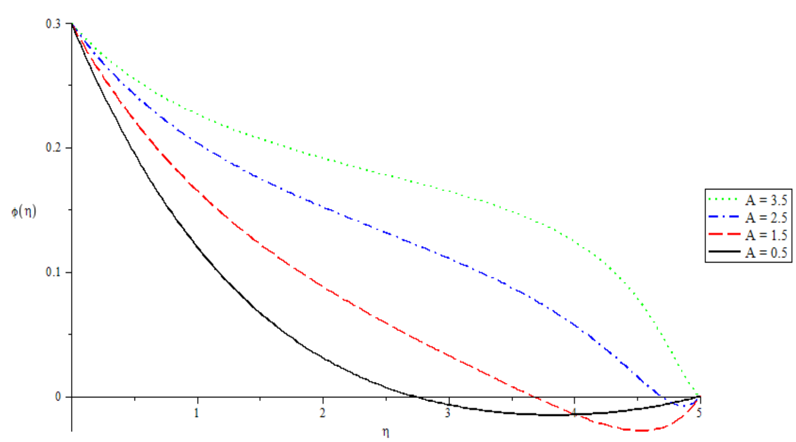

Figure 19: Variation of unsteadiness parameter (A) on concentration profile

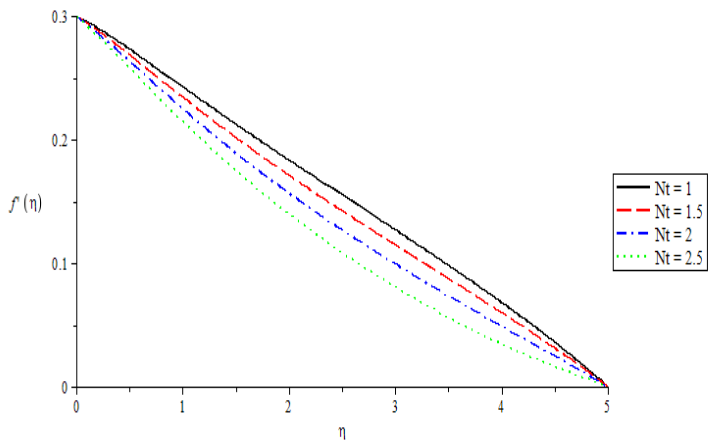

Figure 20: Variation of thermophoresis (N_t) on velocity profile

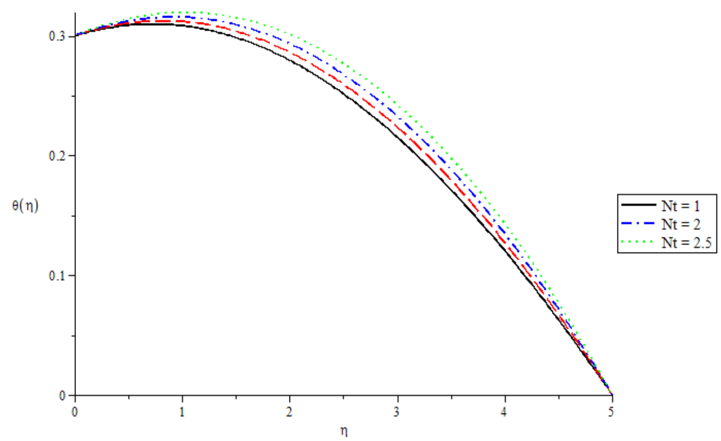

Figure 21: Variation of thermophoresis (N_t) on temperature profile

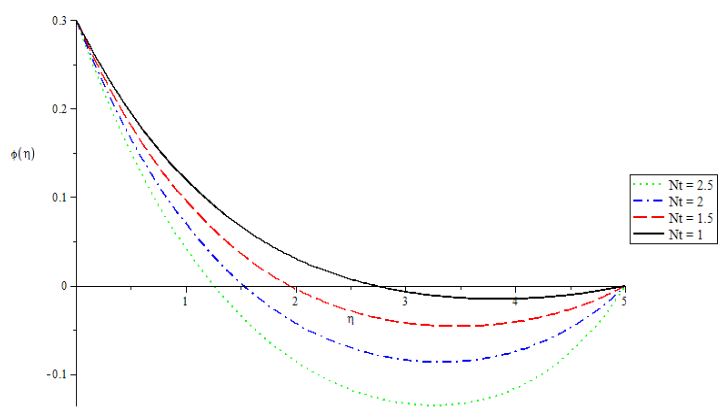

Figure 22: Variation of thermophoresis (N_t) on concentration profile

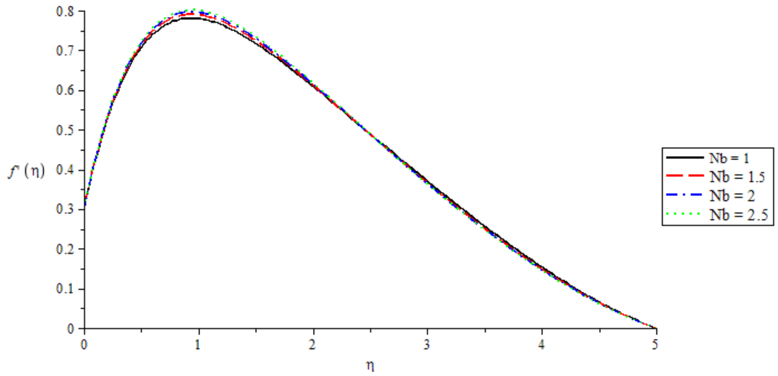

Figure 23: Variation of Brownian motion (N_b) on velocity profile

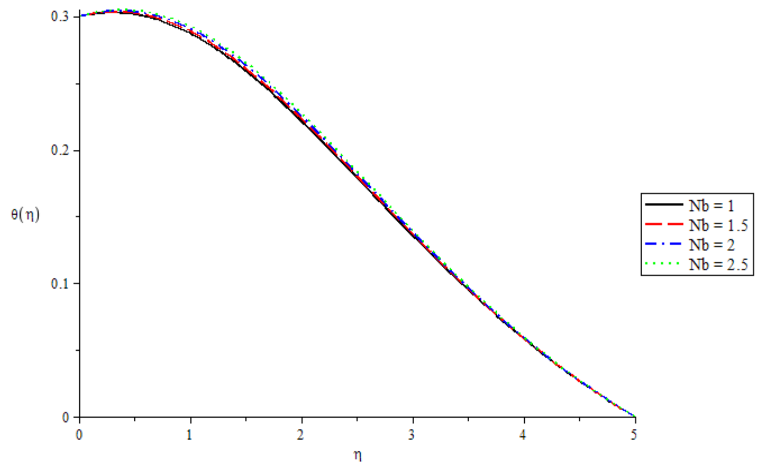

Figure 24: Variation of Brownian motion (N_b) on temperature profile

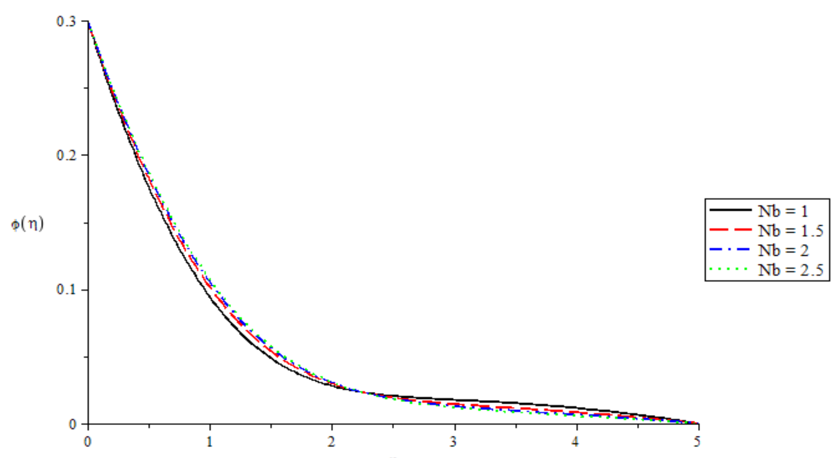

Figure 25: Variation of Brownian motion (N_b) on concentration profile

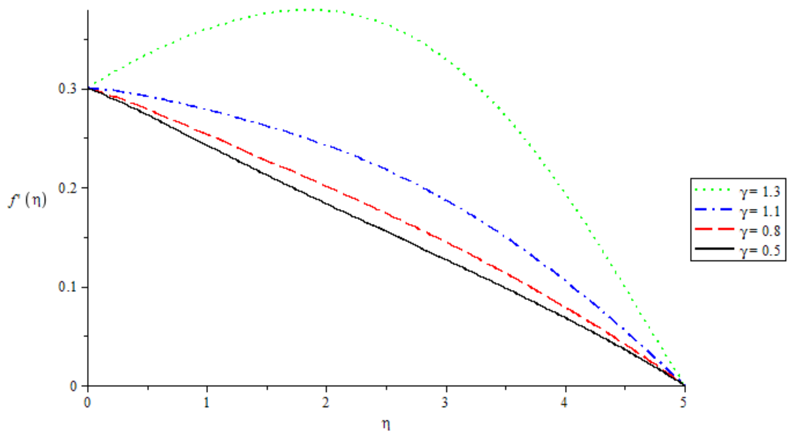

Figure 26: Variation of heat source (γ) on velocity profile

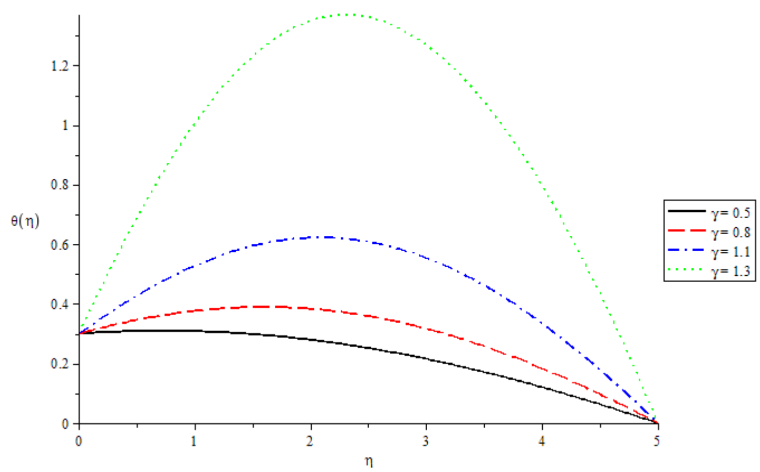

Figure 27: Variation of heat source (γ) on temperature profile

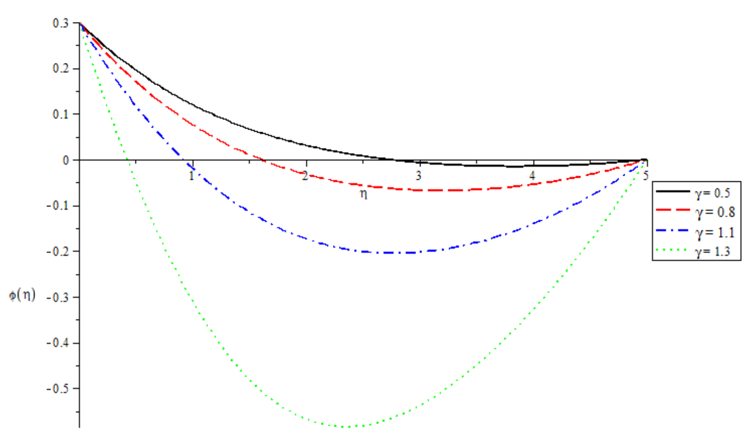

Figure 28: Variation of heat source (γ) on concentration profile

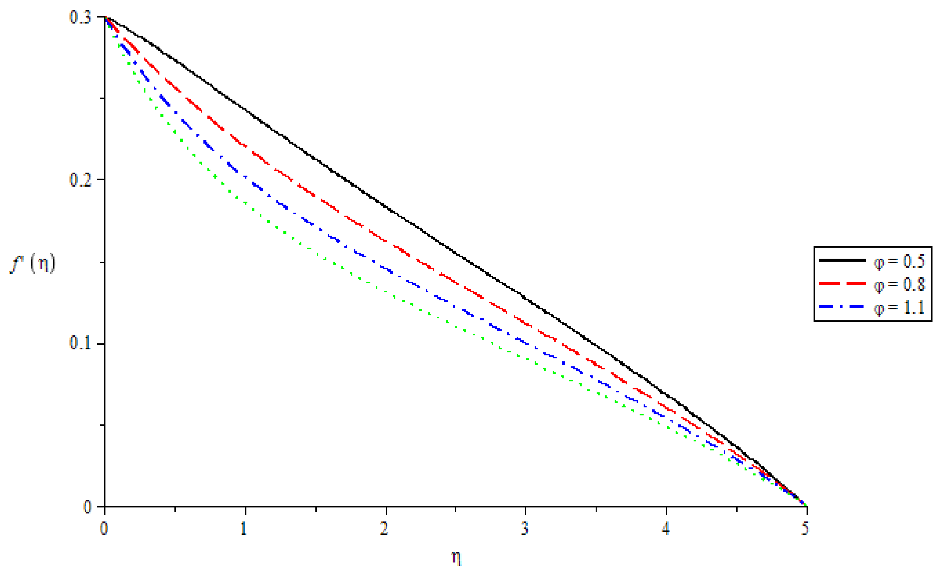

Figure 29: Variation of porous medium parameter (φ) on velocity profile

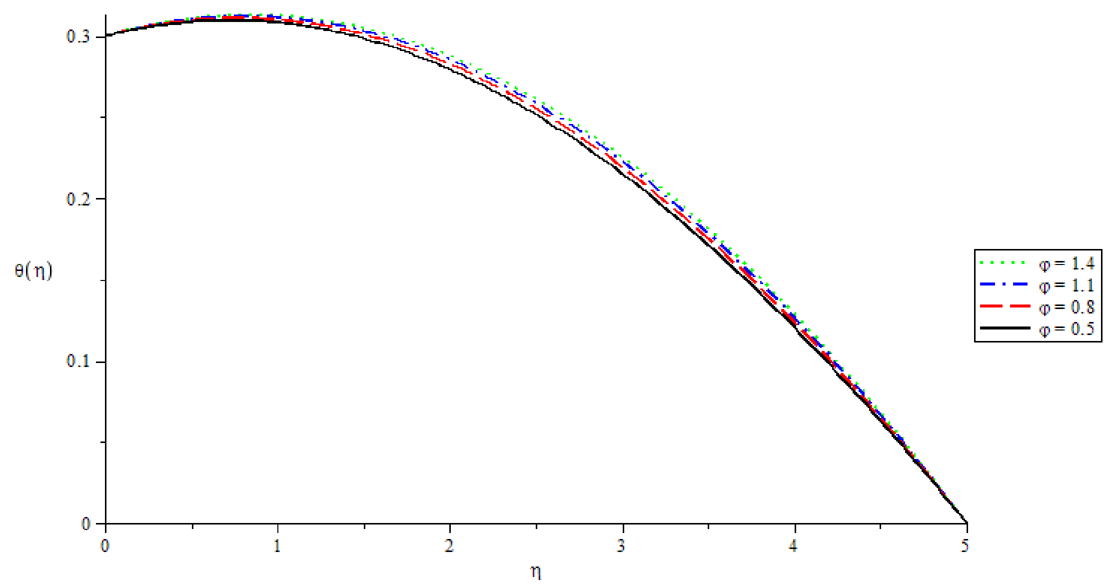

Figure 30: Variation of porous medium parameter (φ) on temperature

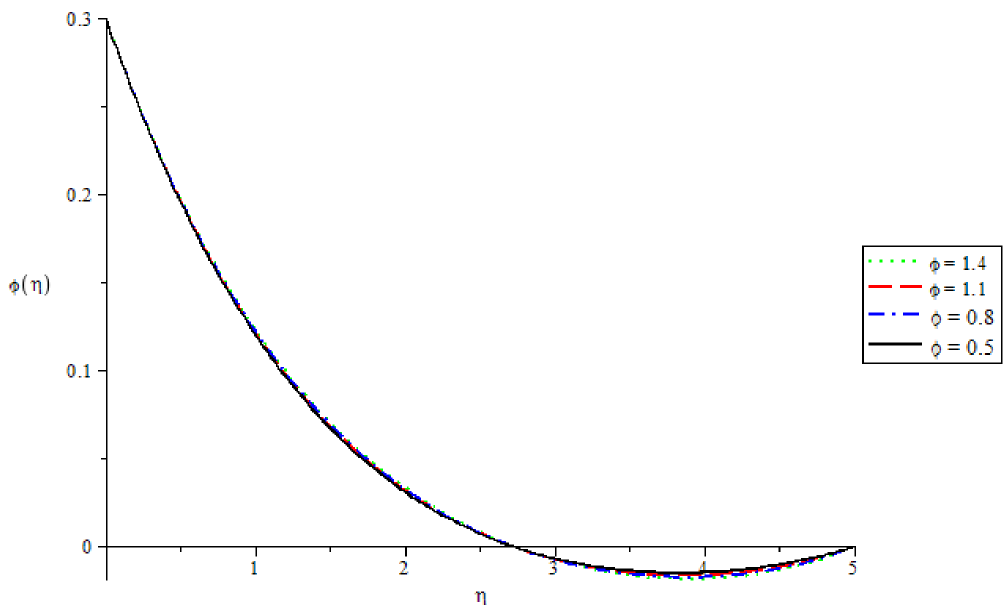

Figure 31: Variation of porous medium parameter (φ) on concentration profile

References

[1] Abbas, W., and Magdy, M. M. (2020). Heat and mass transfer analysis of nanofluid flow based on Cu, Al_2O_3, and TiO_2 over a moving rotating plate and impact of various nanoparticle shapes. Mathematical Problems in Engineering, 2020:1-12.

[2] Pandey, A. K., and Kumar, M. (2017). Chemical reaction and thermal radiation effects on a boundary layer flow of nanofluid over a wedge with viscous and Ohmic dissipation. 10(4):54-72.

[3] Amoo, S.A and Idawo, A.S. (2018) Cross-diffusion effects on heat and mass transfer of MHDs flow in porous media over exponentially-stretching surface. In the flow trends in Science and Technology journal e-ISSN: 2405162; P-ISSN: 20485170. 3(2A) 450-460 www.fstsjournal.com

[4] Bejawada, S. G., and Yanala, D. R. (2021). Finite element Soret Dufour effects on an unsteady MHD heat and mass transfer flow past an accelerated inclined vertical plate. Heat Transfer, 50(8):8553-8578.

[5] Dey, B., Kalita, B., and Choudhury, R. (2022). Radiation and chemical reaction effects on unsteady viscoelastic fluid flow through porous medium. Frontiers in Heat and Mass Transfer (FHMT), 18.

[6] Ganesh, G., and Sridhar, W. (2021). Numerical approach of heat and mass transfer of MHD Casson fluid under radiation over an exponentially permeable stretching sheet with chemical reaction and hall effect. Frontiers in Heat and Mass Transfer (FHMT), 16.

[7] Gharami, P. P., Arifuzzaman, S. M., Reza-E-Rabbi, S., Khan, M. S., and Ahmmed, S. F. (2020).

Analytical and numerical solution of viscous fluid flow with the effects of thermal radiation and chemical reaction past a vertical porous surface. Journal homepage: http://iieta. org/journals/ijht, 38(3):689-700.

[8] Tlili, I., Samrat, S. P., and Sandeep, N. (2021). A computational frame work on magnetohydrodynamic dissipative flow over a stretched region with cross diffusion: Simultaneous solutions. Alexandria Engineering Journal, 60(3):3143-3152.

[9] Sheikholeslami, M., Jafaryar, M., Gerdroodbary, M. B., and Alavi, A. H. (2022). Influence of novel turbulator on efficiency of solar collector system. Environmental Technology & Innovation, 26:102383.

[10] Khan, M. S., Mei, S., Shabnam, Fernandez-Gamiz, U., Noeiaghdam, S., and Khan, A. (2022). Numerical simulation of a time-dependent electroviscous and hybrid nanofluid with Darcy-Forchheimer effect between squeezing plates. Nanomaterials, 12(5):876.

[11] Mabood, F., Shafiq, A., Khan, W. A., and Badruddin, I. A. (2022). MHD and nonlinear thermal radiation effects on hybrid nanofluid past a wedge with heat source and entropy generation. International Journal of Numerical Methods for Heat & Fluid Flow, 32(1):120-137.

[12] Mishra, S. R., Tinker, S., and Sharma, R. P. (2022). Study of a nonuniform heat source over a Riga plate using nth-order chemical reaction on Oldroyd-B nanofluid flow for two-dimensional motion. Heat Transfer, 51(2):1257-1274.

[13] Mulinti, V. R., and Pallavarapu, L. (2021). Influence of thermal radiation and viscous dissipation on MHD flow of UCM fluid over a porous stretching sheet with higher order chemical reaction. Special Topics & Reviews in Porous Media: An International Journal, 12(4).

[14] Khan, N., Ali, F., Arif, M., Ahmad, Z., Aamina, A., and Khan, I. (2021). Maxwell nanofluid flow over an infinite vertical plate with ramped and isothermal wall temperature and concentration. Mathematical Problems in Engineering, 1-19.

[15] Pavar, P., Krishna, L. H., and Reddy, M. S. (2020). Mhd flow of nano fluid past a vertical permeable semi-infinite moving plate with constant heat source. In AIP Conference Proceedings 2246(1). AIP Publishing.

[16] Biswas, R., Hossain, M. S., Islam, R., Ahmmed, S. F., Mishra, S. R., and Afikuzzaman, M. (2022). Computational treatment of MHD Maxwell nanofluid flow across a stretching sheet considering higher-order chemical reaction and thermal radiation. Journal of Computational Mathematics and Data Science, 4:100048.

[17] Shafiq, A., Çolak, A. B., Sindhu, T. N., Al-Mdallal, Q. M., and Abdeljawad, T. (2021). Estimation of unsteady hydromagnetic Williamson fluid flow in a radiative surface through numerical and artificial neural network modeling. Scientific reports, 11(1):14509.

[18] Shafiq, A., Çolak, A. B., Sindhu, T. N., Al-Mdallal, Q. M., and Abdeljawad, T. (2021). Estimation of unsteady hydromagnetic Williamson fluid flow in a radiative surface through numerical and artificial neural network modeling. Scientific reports, 11(1):14509.

[19] Shafiq, A., Lone, S. A., Sindhu, T. N., Al-Mdallal, Q. M., and Rasool, G. (2021). Statistical

modeling for bioconvective tangent hyperbolic nanofluid towards stretching surface with zero mass flux condition. Scientific Reports, 11(1):13869.

[20] Sharma, R. P., Prakash, O., Rashidi, I., Mishra, S. R., Rao, P. S., and Karimi, F. (2022). Nonlinear thermal radiation and heat source effects on unsteady electrical MHD motion of nanofluid past a stretching surface with binary chemical reaction.
The European Physical Journal Plus, 137(3):297.

[21] Sharma, R. P., and Shaw, S. (2022). MHD Non-Newtonian fluid flow past a stretching sheet under the influence of non-linear radiation and viscous dissipation. Journal of Applied and Computational Mechanics, 8(3):949-961.

[22] Reddy, K. S., Reddy, D. B., Triveni, B., Raju, G. S. S., and Raju, M. C. (2020). Analysis of heat and mass transfer flow of nano fluid in conducting field through a vertical plate in porous medium. In AIP Conference Proceedings (Vol. 2246, No. 1, p. 020109). AIP Publishing LLC.

[23] Sulochana, C., Kumar, M. K., and Sandeep, N. (2015). Radiation and chemical reaction effects on MHD thermosolutal nanofluid flow over a vertical plate in porous medium. Chemical and process engineering research, 34:28-37.

[24] Sravan Kumar, T., Dinesh, P. A., and Makinde, O. D. (2020). Impact of Lorentz force and viscous dissipation on unsteady nanofluid convection flow over an exponentially moving vertical plate. Mathematical Models and Computer Simulations, 12:631-646.

[25] Anwar, T., Kumam, P., Shah, Z., Watthayu, W., and Thounthong, P. (2020). Unsteady radiative natural convective MHD nanofluid flow past a porous moving vertical plate with heat source/sink. Molecules, 25(4):854.

[26] Kebede, T., Haile, E., Awgichew, G., and Walelign, T. (2020). Heat and mass transfer in unsteady boundary layer flow of Williamson nanofluids. Journal of Applied Mathematics, 1-13.

[27] Thumma, T., Mishra, S. R., Abbas, M. A., Bhatti, M. M., and Abdelsalam, S. I. (2022). Three-dimensional nanofluid stirring with non-uniform heat source/sink through an elongated sheet. Applied Mathematics and Computation, 421:126927.

[28] Tinker, S., Mishra, S. R., Pattnaik, P. K., and Sharma, R. P. (2022). Simulation of time-dependent radiative heat motion over a stretching/shrinking sheet of hybrid nanofluid: Stability analysis for dual solutions. Proceedings of the Institution of Mechanical Engineers, Part N: Journal of Nanomaterials, Nanoengineering and Nanosystems, 236(1-2):19-30.

[29] Tlili, I. (2021). Impact of thermal conductivity on the thermophysical properties and rheological behavior of nanofluid and hybrid nanofluid. Mathematical Sciences, 1-9.

[30] Rajesh, V., Sheremet, M. A., and Öztop, H. F. (2021). Impact of hybrid nanofluids on MHD flow and heat transfer near a vertical plate with ramped wall temperature. Case Studies in Thermal Engineering, 28:101557.

[31] Zigta, B. (2019). Thermal radiation, chemical reaction and viscous dissipation effects on unsteady MHD flow of viscoelastic fluid embedded in a porous medium. Budapest International Research in Exact Sciences (BirEx) Journal, 1(3):35-57.